C. 2

Copy 6

RM E53H27

NACA RM E53H27

RESEARCH MEMORANDUM

PERFORMANCE OF A SUPERSONIC MIXED-FLOW ROTOR WITH A SWEPT LEADING EDGE AND 0.52 INLET RADIUS RATIO

By Arthur W. Goldstein and Ralph L. Schacht

Lewis Flight Propulsion Laboratory
Cleveland, Ohio

NATIONAL ADVISORY COMMITTEE
FOR AERONAUTICS

WASHINGTON

November 20, 1953

NACA RM E53H27

NATIONAL ADVISORY COMMITTEE FOR AERONAUTICS

RESEARCH MEMORANDUM

PERFORMANCE OF A SUPERSONIC MIXED-FLOW ROTOR WITH A SWEPT LEADING EDGE AND 0.52 INLET RADIUS RATIO

By Arthur W. Goldstein and Ralph L. Schacht

SUMMARY

A 14-inch supersonic mixed-flow rotor of high specific mass flow and an inlet radius ratio of 0.52, designed for impulse operation and uniform work output, was tested in Freon-12.

For operation without strong internal shocks (impulse operation) at design tip speed (686 ft/sec in Freon-12, 1480 ft/sec in air), the pressure ratio, adiabatic efficiency, and equivalent weight flow were, respectively, 7.2, 76.9 percent, and 63.8 pounds per second (equivalent air value, 31.5 lb/sec/sq ft frontal area). At 70 percent of design speed, these parameters had the values 2.9, 84.0 percent, and 51.1 pounds per second. With shock-in-rotor operation, large variations in weight flow were obtainable without audible surge. The minimum speed at which impulse operation was obtained was 68 percent of design speed.

Friction with the casing appeared to be a substantial factor affecting efficiency at 90 and 100 percent of design speed. The remainder of the losses were nearly constant at 13 percent of the work input for all speeds at impulse operation. Exit surveys showed that exclusive of casing friction, the high loss gas was concentrated principally near the casing with some additional losses near the roots.

The angle of attack at the entrance was large at the blade roots and small or negative at the tips. Further, the blade roots at the entrance gave rise to a system of pressure waves which affected the pressure and flow direction upstream of the rotor at the tips and therefore affected the pressure distribution in the initial portion of the rotor. Downstream of this initial section, the flat pressure distribution calculated by the assumption of axially symmetric flow was found to be only roughly correct at design speed.

A high efficiency for impulse operation occurred at 70 percent of design speed where the pressure variations along the casing were the greatest.

INTRODUCTION

The present paper is a continuation of a project first reported in reference 1 - exploration of the aerodynamic problems in developing a supersonic compressor with shockless flow in the rotor attaining a pressure ratio in the region of 6 to 10 and nearly the maximum possible air flow per unit frontal area. For a single rotor in this pressure ratio range, a supersonic flow is required; and it is believed that the diffusion problems are best handled in the stationary diffuser where variable geometry passages and other devices not feasible in a rotor may be used. The program is to be continued into the diffuser problem.

The rotor to be discussed herein is identical to that reported in reference 1 except that the design weight flow was increased from 21.6 to 31.9 pounds of air per second per square foot frontal area by reducing the inlet radius ratio from 0.71 to 0.52.

The purpose of this study is to obtain the operating characteristics of the rotor as well as specifically (1) to find the accuracy of the axisymmetric design method by comparing the static pressures at the rotor casing and flow surveys with those computed in the design process, (2) to find the effect of radius ratio by comparison of performance of the rotors having 0.71 and 0.52 inlet radius ratios, (3) to obtain more data for correlation of rotor efficiency and casing friction, (4) to find whether the design method for equalizing the work input to the gas was adequate for the rotor with the 0.52 inlet radius ratio, (5) to find whether the expected high mass flows would be realized, and (6) to find whether the higher diffusion rates on the hub of the rotor having a 0.52 inlet radius ratio would cause deterioration of the internal flow near the hub.

EQUIPMENT AND PROCEDURE

Rotor design. - The rotor was designed to operate in Freon-12 at an isentropic pressure ratio of about 8.0, an equivalent tip speed of 686 feet per second, and an axial inflow Mach number of about 0.85. The hub and casing were cylindrical for zero radial velocity at the rotor inlet, and guide vanes were set for a free vortex rotating counter to the direction of wheel rotation. Inlet and outlet velocity diagrams for root and tip sections are shown in figure 1.

The internal flow was to be shockless. Relative discharge flow direction was to be approximately axial. Effectively, subsonic leading edges of the blades were obtained by sweeping the tip back for subsonic normal gas velocities. Work output was equalized at the exit by sweeping the trailing edge back to provide additional blade surface at the root for work input to the gas.

The blade tip camber line was determined by a surface velocity distribution such that the mean channel velocity was equal to the entrance value (950 ft/sec), and the suction surface velocity had a maximum value of 1120 feet per second over most of the profile. Camber lines at other radii were determined by radial projections of the tip. To these camber lines were added 1/8 inch total normal blade thickness. A small region near the trailing edge is nonradial. Leading edges are rounded, and trailing edges are sharpened to a 16.5° wedge. Axially symmetric flow (infinite number of blades) was assumed, and the internal flow was then calculated according to the method of reference 2. (A summary of details in procedure is given in ref. 1.) Any particular streamline was then selected for the hub. (In this particular case the streamline intersecting the leading edge at a radius ratio of 0.52 was selected, while a value of 0.71 was chosen for the rotor reported in ref. 1.) Allowance was made on the hub for estimated boundary-layer growth.

The coordinates of the blade surface and the hub contour which resulted from this design process are given in table I.

A picture of the rotor is shown in figure 2.

Figure 3 shows an outline of the hub, the calculated characteristic network, and Mach number contours for the axisymmetric flow obtained in the design process.

Test rig. - The test rig installation and measuring stations are the same as described in reference 1 and are shown in figure 4. The impeller was tested with Freon-12 as the working fluid in a closed circuit, as shown in figure 5.

Inlet stagnation temperatures and pressures were measured in the surge tank. Four static taps in the inlet nozzle were used for determining the flow; these were calibrated by numerous surveys of weight flow made at station 1. At station 1, three claw probes were used with four pressure taps on the hub and four on the casing. Exit-survey instruments used are shown in figure 6. For detailed surveys three wedge-type pressure probes (fig. 6(a)) at station 3 and six semishielded thermocouple probes (fig. 6(c)) at station 4 were used; for over-all performance measurements six radially fixed claw probes were used at station 3 with the six thermocouple probes at station 4. The calculations and the procedure for testing the rotor were carried out in the same manner as with the previous rotor.

Two of the instruments used were new in this series of tests. One of these is a wedge with side static-pressure taps and total-pressure probes (fig. 6(a)). With this instrument it is possible to find the Mach number, direction of flow, and total pressure of the fluid at any point in the flow field. For use in Freon-12 in the Mach number range of

interest (greater than 1.8), a 17° semiwedge angle was used and found satisfactory. This instrument obviates the very large corrections necessary for a normal shock instrument which gives results very sensitive to errors in the stream static pressure; the wedge instrument requires correction for an oblique shock followed by a normal shock, which is a more efficient process than a single normal shock.

The static-pressure distribution at station 3 as determined from the wedges gave curves consistent with static pressure at the inner and outer walls found from wall taps. The wall tap pressures were always determined with all instruments retracted from the stream because the presence of the instruments was found to interfere with the readings. This particular wedge design is ineffective for Freon-12 with Mach numbers less than 1.8 and therefore for exit measurements with strong shock in the rotor, the well-known claw probes (fig. 6(b)) were used with static pressures interpolated linearly between wall tap readings.

An indication of the accuracy of the pressure measurements at station 3 is obtained by comparison of the weight flow computed from surveys at the exit and that from surveys at the inlet. The weight flows as determined at impulse operation from entrance surveys at design speed and at 90 percent of design speed were 63.8 and 62.7 pounds of Freon-12 per second, respectively. The exit survey values as obtained from the wedge probe were 63.2 and 62.2 pounds of Freon-12 per second, respectively, which indicates agreement within 1 percent in weight flow and 1 percent error in the static and total pressures if these two are assumed to have equal errors. For shock-in-rotor operation, the calculation of equivalent weight flow from claw-probe data and wall tap readings showed random variations of 2 to 3 percent from inlet survey values. This indicates errors in the pressure of from 2 to 3 percent.

The second new instrument used was a semishielded thermocouple probe (fig. 6(c)), which was devised to register good recovery and also to provide scrubbing of the junction by the normal turbulence of the gas discharged from the rotor. This instrument gave better agreement between surveys of the temperature at station 3 and station 4 than did the double-shielded thermocouple (fig. 6(d)) at design speed and was therefore used in the calculation of rotor performance. Temperature data obtained at station 4 were used in all calculations.

An unexplained discrepancy was obtained between the dynamometer readings and temperatures at 90 percent of design speed and full speed for impulse operation. Temperature surveys indicated an increase in enthalpy of the gas of 18.7 and 23.8 Btu per pound at 90 percent of design speed and full speed, respectively, whereas the dynamometer readings indicated 17.8 and 22.2 Btu per pound for the same speeds. This corresponds to temperature errors of +5.5° and +9.5° F, respectively, or errors in the power as determined from the dynamometer of -5 and -6.5 percent.

The efficiencies reported were calculated from the temperatures, although there was no indication that the temperatures were more reliable than the dynamometer readings.

The performance of this impulse-type supersonic compressor rotor was determined over a range of back pressure from open throttle to near audible surge at six wheel speeds from the design value (686 ft/sec in Freon-12) to 50 percent of the design value. The inlet tank pressure was maintained at 15 inches mercury absolute during all tests, and temperature varied from 80° F to 150° F, depending on the load on the cooling system. Freon purity was maintained over 97 percent.

RESULTS AND DISCUSSION

Over-All Rotor Performance

The rotor was found to operate in either of two modes at 68 percent of design speed or higher. In the first mode a strong shock was located in the impeller and caused a relative subsonic velocity inside. As the throttle was opened the weight flow increased to a point where the internal shock passed from the leading edge through the rotor, so that the relative internal velocities became supersonic. With this discontinuous change in mode from shock-in-rotor to impulse operation, the weight flow remained practically unchanged; but the pressure ratio, the efficiency, and the equivalent specific stagnation enthalpy rise ΔH_e of the gas all changed discontinuously to higher values.

The over-all performance of the rotor in terms of weight flow, ΔH_e, pressure ratio, and efficiency for various speeds is shown in figure 7. The most significant values (those for impulse operation) are summarized in the following table:

N/N_D	W_e	ΔH_e	$p_{T,3}/p_{T,0}$	η_{ad}, percent
0.70	51.1	11.0	2.9	84.0
.80	55.4	13.9	3.8	85.9
.90	62.7	18.7	5.2	80.9
1.00	63.8	23.8	7.2	76.9
1.00[a]	64.7[a]	19.9[a]	---	----

[a]Design value.

where

N/N_D ratio of rotative speed to design value, N_D = 11,220 rpm for standard inlet temperature

W_e equivalent mass flow of gas, lb/sec

[redacted]

p_T stagnation pressure

Subscript 3 indicates station 3; subscript 0 refers to inlet tank.

The equivalent enthalpy rise was computed by means of

$$\Delta H_e = \frac{T_n}{T_{T,0}} \Delta H$$

(The equivalent enthalpy rise ΔH_e is the value of H which will be obtained with standard inlet conditions.)

where

T_n standard temperature, 518° R

T_T stagnation temperature

ΔH increase in stagnation specific enthalpy from station 0 to station 4

The efficiency was calculated from

$$\eta_{ad} = \frac{\Delta H_{is}}{\Delta H}$$

where

ΔH_{is} increase in specific enthalpy at constant entropy from $p_{T,0}$ to $p_{T,3}$

(A summary of all symbols used in the report is given in the appendix.)

A range of gas flow which is large for a high-pressure-ratio machine is obtainable without encountering audible surge (fig. 7(a)). At 50 percent of design speed, the ratio of maximum to minimum flow was 2.3, and at full speed the ratio was about 1.14. At the high flow end the jump in enthalpy rise may be explained from the fact that the blades are turned forward at the root and the increase in discharge velocity, which occurs when the shock is swallowed, causes an increased rotational component of velocity of the discharged gas and therefore also an increase in work input to the gas. At 100 percent speed the jump was about 3.7 Btu per pound as compared with 2.0 Btu per pound for the 0.71 inlet radius ratio machine. This difference is to be expected because the forward turning section of the blade roots is not as extensive in the 0.71 radius ratio rotor as in the 0.52 inlet radius ratio rotor. The lowest speed at which

the internal shock is passed through the rotor was found to be 68 percent of design, whereas in the 0.71 inlet radius ratio rotor the lowest speed was 60 percent design speed. Shock losses and separation losses will reduce when transition to impulse operation occurs, and the efficiency will rise, as shown in figure 7(b). At 100 percent speed the total loss $(1-\eta_{ad})\Delta H_e$ with shockless operation amounted to 62 percent of the losses for shock-in-rotor operation; and at 70 percent, the losses were reduced to 43 percent of the losses for shock-in-rotor operation. Therefore, in transition from internal shock to impulse operation, the pressure ratio increased because of the rise in work input to the gas and also because of the reductions in internal losses (see fig. 7(c)).

Weight flows of the present rotor and of the low flow rotor were near the design value. The efficiencies were also nearly equal, but the specific enthalpy rise was about 4 percent higher for the present rotor.

Casing Friction

The moment of momentum of the gas passing through the rotor is increased by the torque exerted by the rotor and decreased by the frictional torque exerted by the casing. Therefore mass flow $\times \frac{\Delta rc_u}{12}$ = wheel torque τ_w - frictional torque τ_f where $\frac{\Delta rc_u}{12}$ is the mass-averaged change in moment of momentum. The power input from the rotor to the gas is $\omega\tau_w$, and this is equal to the specific enthaly rise ΔH times the mass flow W, so that

$$\frac{\omega\tau_f}{W} = Jg\Delta H - \omega\frac{\Delta rc_u}{12}$$

gives the increment in specific work required because of casing friction, where

J mechanical equivalent of heat, 778.26 ft-lb/Btu

g ratio of pounds force to poundals force, 32.174

ω angular velocity of rotor, radians/sec

Casing friction work was computed for impulse operation in two ways: the term $JW\Delta H$ was determined from the change in stagnation state of the gas and the weight flow (indicated by subscript m) and also from the wattmeter readings (indicated by subscript w) corrected for losses in

the motor, gears, and bearings. The ratio of casing friction loss to work input is represented by F; the symbol L is used to indicate all losses other than those resulting from casing friction and was calculated from the formula

$$L = \frac{\omega \Delta r c_u}{12} - \Delta H_{ls}$$

The dynamometer power corrected for regular losses is in Btu per second and is represented by P. The inlet relative kinetic energy of the gas in Btu per pound is represented by K.E.

N/N_D	0.70	0.80	0.90	1.00
F_m	0.03	0.02	0.07	0.09
F_w	.01	.04	.03	.04
$L/\Delta H$	.13	.13	.12	.14
$L/P/W$	.13	.13	.13	.15
L/K.E.	.21	.19	.19	.23

There is considerable uncertainty as to the amount of loss resulting from casing friction, but both methods indicate that this loss, as for the low flow rotor, is of considerable magnitude. Exclusive of casing friction work, the specific work inputs of both rotors are equal. The quantities $L/\Delta H$ and $L/(P/W)$ are ratios, the numerators of which are the same functions of the pressures and depend only slightly on the temperature determination, whereas the denominators are the work input per pound of gas. Consequently, $L/\Delta H$ and $L/(P/W)$ are nearly equal. The approximate constancy of these functions indicates that if casing friction were negligible, the rotor might be expected to have an approximately constant efficiency of 87 percent for impulse operation at all speeds. Losses other than casing friction are approximately 20 percent of the inlet relative kinetic energy at all speeds. (In consideration of the limits on the accuracy of the data, the increase of 4 percent in kinetic energy loss at design speed ($L/\Delta H$ indicates that this corresponds to an efficiency decrease of only 2 percent) is not considered to be of significant magnitude.)

Entrance Flow

A plot of the relative inflow Mach numbers at station 1 is shown in figure 8(a), which also includes the data from the 0.71 inlet radius ratio impeller. (The operating points on all figs. in this report are indicated by numbers which designate the ratio of speed to design speed and the letter I or S, which indicates either impulse or shock-in-rotor condition.)

[redacted]

The Mach numbers at all radii were about 0.05 higher than design value at full speed and decreased uniformly with rotor velocity. The relative flow angles, shown in figure 8(b), agree very well at 100 and 90 percent of design speed with the estimated value at the tip for station 1, but are higher at smaller radii.

Figure 9(a) shows a drop in pressure between station 1 (about 4.1 in. upstream of the blade tip) and the impeller tip at design speed. This causes an acceleration of the flow component of velocity and a change in the direction of flow. The change is negligible at the root because the sweepback of the leading edges places the blade roots close to station 1. Calculation of the modified relative flow direction and magnitude by means of the pressure drop gave the results shown in figures 8(a) and 8(b) at the 7-inch radius. At design speed the relative Mach number was increased from the design value of 1.91 to 2.10, the value at 90 percent of design speed remains unchanged at 1.74, and at 70 percent of design speed the Mach number increases from 1.29 to 1.42. The angle of attack (angle between leading edge camber lines and relative velocity vector) with respect to the tip of the blades at design speed was changed from 4° to -3°, whereas the estimated value was 4°. At 90 percent of design speed the tip angle of attack remained unchanged at 3.5°, while at 70 percent the angle changed from 7.8° to -1.0°. At the root the angle of attack was high for all speeds - 13.5° at 70 percent speed and 11.5° at full speed. At full speed the flow direction at the pitch section was approximately equal to the estimated upstream direction, although error in the estimate is large at the root (-4°) and at the tip ($+7^\circ$). These variations of angle of attack with speed do not appear to be significant because the losses are a nearly constant percentage of inlet kinetic energy.

From analysis of the data from the 0.71 radius ratio rotor (ref. 1), it was found that the relative flow angle was set by the rotor blade shape near the leading edge. For the two rotors, the differences in inflow conditions must be ascribed to the effect of the root section on the gas inflow in other regions, since the blade shapes are identical for inlet radii greater than 0.71 of the tip radius.

Distribution of Static Pressure on Casing

The design conditions (impulse operation) for both the 0.71 and 0.52 inlet radius ratio impellers specified a uniform pressure along the casing, but the data for the 0.52 radius ratio impeller showed a drop to 73 percent of design value at the entrance and to 77 percent at $z = 6.5$ inches (fig. 12). The data for the 0.71 impeller showed a drop to 82 percent of the design value at several regions. These deviations are a measure of the accuracy of the axisymmetric assumption in calculating internal flow. A good basis for comparing the casing pressure curves of the two rotors

[redacted]

is obtained by referring both to the static pressure at station 1, in which case the lowest curve would be raised in the ratio 0.71/0.64, and the curves for both rotors would show good agreement except at the entrance (3.0 in. < z < 3.5 in.). This difference in observed pressure distribution is related to the observed differences in inlet angle and Mach number discussed in the previous section, and indicated that the assumption of axially symmetric flow is in need of refinement for calculating the factors determining the induction process.

The drop in casing pressure between station 1 (z = -0.75 in.) and the rotor caused a change in flow so that the gas impinged on the blade at a negative angle of attack. Once the gas has entered the rotor, an estimate of pressure variation may be made on the assumption of turning to the blade direction. The result of this calculation was a static pressure of 0.63 $p_{T,0}$, which closely checks the static-pressure rise observed. It may therefore be said that the initial pressure rise at the blade tips resulted from adjustment of the flow from the external flow, and therefore ultimately was caused by the exterior pressure drop initiated by the leading edges near the hub.

The design calculations gave the Mach number contours of figure 3. There is a Mach number decrease at the root from 1.55 to 1.2 at z = 3.1 inches, and an increase from that point on. There was a possibility that this velocity decrease might cause separation. If separation did occur, it would cause a pressure rise starting at z between 2 and 3 inches on the hub to be transmitted along a characteristic to the tip at z between 4 and 4.5 inches, so that the final pressure there would be greater than the upstream value of 0.64 $p_{T,0}$, since the rise from z = 3.5 to 4.25 inches has already been accounted for. Because this pressure rise is not apparent, it is believed that separation did not occur at this point.

Closing the throttle sufficiently to cause a slight reduction in weight flow forced a shock into the rotor, increased the discharge static pressure, and reduced the discharge velocity. The initial compression shock could not be stabilized inside the impeller at any position other than the leading edge. A pressure distribution on the casing for such a mode of operation is shown in figure 9(b). Because the rate of pressure rise is not high enough for a simple normal shock, it is believed that either separation and reacceleration are taking place (as is observed in ducts with appreciable boundary layer), or a strong oblique shock is located at the entrance to the impeller. The curve is practically coincident with that for the 0.71 radius ratio impeller for which the same conclusion was reached.

If the pressure distributions for impulse operation at various speeds are examined (fig. 9(a)), it is seen that in the initial portion of the

blades $\left(3\frac{3}{8} \text{ in.} < z < 4\frac{1}{2} \text{ in.}\right)$ there was a pressure rise at design speed, a constant pressure at 90 percent speed, and a decreasing pressure at 70 percent speed. As originally conceived, a desirable feature of good design for efficient rotor operation was thought to be constant or decreasing pressure at the casing. Figure 9(a) shows that this is not a requirement for efficient operation with supersonic discharge velocity because at 70 percent of design speed where the efficiency was close to the maximum there was a large initial pressure drop followed by a rise with a ratio of 1.65.

At all speeds there was a pressure rise near the back end of the rotor. At 70 percent of design speed the steepest compression started at about $z = 7.0$ inches, and at high speeds it was displaced backward (as might be expected if the shock were transmitted from the hub with decreasing wave angle as the Mach number increased) to $z = 7.8$ inches at 90 percent of full speed; at full speed the pressure rise appears to be more gradual, but seems to be located somewhat downstream of $z = 8.0$ inches. If the characteristic is traced from $z = 8$ inches back to the hub at $z = 5$ inches, there appears to be no reason (either from separation or hub contour effect) for the origin of the shock on the hub, because the design calls for a pressure drop and no boundary concavity exists there. It therefore appears likely that the pressure wave was reflected from the hub and originated upstream, possibly from the process of induction of gas into the rotor. The calculations for axially symmetric flow give no insight into the origin of this wave.

Exit Flow

At the exit the discharged gas had the loss distribution (exclusive of casing friction loss) shown in figure 10(a). The relatively large loss evident in the gas discharged near the tip results from losses which occurred at the blade tips as well as from centrifuged blade boundary layer. Most of the loss which occurred near the blade roots did not centrifuge out beyond $r = 6.4$ inches, as indicated by the minimum loss region at this radius. The importance of the losses is shown by the adiabatic efficiency distribution in figure 10(b), which includes the distributed casing friction loss because these calculations are based on temperature readings at station 4.

Relative discharge angles (fig. 10(c)) indicate an overturning of about 4° in the center of the blade span. This overturning was observed in the 0.71 radius ratio impeller and presents the same unexplained problem as before, inasmuch as both impellers are designed for a loading which decreases to zero at the trailing edge.

A comparison of the measured and estimated relative discharge Mach number is shown in figure 10(d). The drop off at the tip and at a radius of 5.65 inches at design speed is a reflection of the large losses in those regions shown in the efficiency distribution (fig. 10(b)). The blades were designed for uniform specific energy input to the gas from root to tip. However, because of friction with the casing, the work input to the gas should be slightly higher than design values, especially near the tip. As an indication of energy input without the effect of casing friction, the distribution of moment of momentum change of the discharged gas is shown in figure 10(e). Only a small variation from the mean (±4 percent) of momentum change is shown by the plot; the work-equalizing property of the blades may therefore be considered satisfactory.

The average equivalent value of $\omega\Delta rc_u$ is 21.5 Btu per pound, which is higher than the design value of 19.9 Btu per pound by about 8 percent. This discrepancy correlates with the overturning of the gas as shown in figure 10(c).

Although the impeller efficiency, pressure ratio, and air-flow capacity make it attractive as a component of a compressor at 70 percent and 80 percent of design tip speed (1040 ft/sec and 1180 ft/sec equivalent air values), there still remain difficult problems for the diffuser design, as plots of the exit Mach number and angle of discharge show (fig. 11). The average Mach number varies from about 1.0 (shock-in-rotor operation, 70 percent of design speed) to 2.4 (impulse operation at full speed), and average angles vary from about 34° (impulse operation at 70 percent speed) to 66° (shock-in-rotor operation at full speed). If a diffuser with a fixed throat area were designed for this rotor, it could be expected to operate effectively at only one rotor condition. Large variations in possible weight flows, which are a feature of the performance of this rotor, may provide needed latitude in starting a diffuser without surging the compressor.

SUMMARY OF RESULTS AND CONCLUSIONS

A 14-inch supersonic mixed-flow rotor with an inlet radius ratio of 0.52, designed for impulse operation and uniform work output, was tested in Freon-12. The following characteristics were determined:

At any speed higher than 68 percent of the design value, two modes of operation were possible: first, with a strong internal shock and subsonic relative discharge velocity, and second, with a supersonic relative discharge velocity. In the low flow impeller (0.71 inlet radius ratio, ref. 1), the lowest speed at which this phenomenon was observed was 60 percent of design speed. In the second mode, only one operating point was obtainable with each speed; while in the first, a large variation of weight flow was possible. As the compressor passed from shock-in-rotor to impulse operation, a large increase in energy input to the gas was

obtained as a result of the increase in discharge velocity and the turning beyond the axial direction of the blades at the root near the trailing edge. An increase in efficiency was also obtained as a result of the improvement of the internal flow. For impulse operation, as the speed was increased from 70 percent to the design value of 686 feet per second, the weight flow increased from 51.1 to 63.8 pounds per second, the pressure ratio increased from 2.9 to 7.2, and the efficiency decreased from 84.0 to 76.9 percent. The design value of weight flow was 64.7 pounds per second - slightly higher than that obtained. The 0.71 radius ratio rotor also delivered close to the design value of weight flow. Design value of work input was 19.9 Btu per pound and the measured value was 23.8 Btu per pound, which was about 20 percent too high and 4 percent higher than for the previously tested rotor. If casing friction is subtracted, the net input to the gas is equal to that for the first rotor - 21.5 Btu per pound, which is about 8 percent too high. The variation of enthalpy rise from root to tip was small enough for both rotors for the swept trailing edges to be regarded as satisfactory in equalizing the work input to the gas.

Friction with the casing caused a considerable loss as it did for the low flow rotor. Other losses were approximately 13 percent of the work input and were nearly a constant percentage (20 percent) of the inlet relative kinetic energy. Either the portion of these losses which occurred at the center of the span was small or the resulting high entropy gas was centrifuged out to the blade tip.

From the pressure distribution on the casing it was inferred that a shock originated at or near the entrance, reflected off the hub, and was observed at the tip. The axisymmetric flow calculations give no insight into the origin of the wave, nor do they give any explanation for the drop in casing pressure to 73 percent of the design value. On the basis of the static pressure at station 1, both rotors had very similar casing pressure distributions for axial distance $z > 3.7$ inches, but showed larger differences for $z < 3.7$ and for a short distance upstream of the leading edge. This indicates an effect of radius ratio and a limitation of the assumption of axially symmetric flow. The diffusion on the hub as determined from design calculations caused no apparent detrimental effects.

Unlike the condition for the 0.71 inlet radius ratio rotor, the flow upstream of the 0.52 radius ratio impeller was altered by the rotor itself; the root section of the blade, which was swept forward, appeared to influence the flow upstream of the tip. The angle of incidence of the inflow, which varied at the tip from -3.0° at design speed to -1.0° at 70 percent of design speed and at the root from 11.5° to 13.5°, did not appear to be significant because the internal losses were constant for all speeds.

Moderate pressure variations (ratio of 1.65) on the casing were found not to interfere seriously with the efficiency of the flow process at 70 percent design speed, where an efficiency of 84.0 percent was obtained.

Lewis Flight Propulsion Laboratory
National Advisory Committee for Aeronautics
Cleveland, Ohio, September 11, 1953

APPENDIX - SYMBOLS

The following symbols are used in this report:

c_u tangential component of absolute velocity of gas, ft/sec

F_m ratio of casing friction loss to work input, $F_m = \frac{\Delta H-(\omega\Delta rc_u)/12}{\Delta H}$

F_w ratio of casing friction loss to work input, $F_w = \frac{P/W-(\omega\Delta rc_u)/12}{P/W}$

g ratio of pounds force to poundals force, 32.174

ΔH increase in specific stagnation enthalpy from station 0 to station 4, Btu/lb

ΔH_{is} increase in specific enthalpy at constant entropy from $p_{T,0}$ to $p_{T,3}$, Btu/lb

J mechanical equivalent of heat, 778.26 ft-lb/Btu

K.E. inlet relative kinetic energy of gas, Btu/lb

L total loss - friction loss, $L = (\omega\Delta rc_u)/12 - \Delta H_{is}$, Btu/lb

M absolute Mach number, ratio of absolute velocity of fluid to local velocity of sound

M' relative Mach number, ratio of velocity of fluid relative to rotor to local velocity of sound

M_A axial Mach number, ratio of axial component of velocity of fluid to local velocity of sound

N/N_D ratio of rotative speed to design value (N_D = 11,220 rpm for standard inlet temperature)

P dynamometer power corrected for rig losses, Btu/sec

p static pressure, lb/sq in.

p_T absolute stagnation pressure, lb/sq in.

r radial distance from axis of rotation, in.

T_n standard temperature, 518.4° T

T_T absolute stagnation temperature, °R

W mass flow of gas, lb/sec

z distance parallel to axis of rotor, in.

α angle between axis of rotation and relative velocity vector, deg

ϵ angle between axis of rotation and absolute velocity vector, deg

η_{ad} adiabatic efficiency of rotor, $\eta_{ad} = \frac{\Delta H_{is}}{\Delta H}$

τ_f frictional torque, poundal-ft

τ_w wheel torque, poundal-ft

ω angular velocity of rotor, radians/sec

Subscripts:

0 entrance tank upstream of nozzle (see fig. 4)

1 station 1 at rotor entrance (see fig. 4)

3 station 2.5 in. downstream of impeller blade (see fig. 4)

4 station 8.0 in. downstream of impeller blade (see fig. 4)

e equivalent value for standard pressure and temperature

2911

REFERENCES

1. Goldstein, Arthur W., and Schacht, Ralph L.: Performance of a Swept Leading Edge Rotor of the Supersonic Type with Mixed Flow. NACA RM E52K03, 1953.

2. Goldstein, Arthur W.: Axisymmetric Supersonic Flow in Rotating Impellers. NACA Rep. 1083, 1952. (Supersedes NACA TN 2388.)

[redacted]

TABLE I. - CYLINDRICAL (POLAR) COORDINATES OF HUB AND BLADE CAMBER LINES[a]

Axial distance, z, in.	Radius, r, in.	Angular coordinate	Axial distance, z, in.	Radius, r, in.	Angular coordinate
0	[b]3.649ht	0	8.00	[c]5.188	73°49.0'
.50	3.674h	8°43.5'		5.250h	73°49.0'
	4.149t	8°43.5'		5.927	73°49.0'
1.00	3.708h	16°56.1'		6.457	73°53.9'
	4.649t	16°56.1'		7.000t	73°28.7'
1.50	3.766h	24°46.7'	8.50	[c]5.188	73°26.9'
	5.149t	24°46.7'		5.225h	73°26.9'
2.00	3.853h	32°21.1'		5.927	73°26.9'
	5.649t	32°21.1'		6.457	73°52.8'
2.50	3.973h	39°43.2'		6.690t	
	6.149t	39°43.2'		[c]7.000	73°51.2'
3.00	4.159h	46°54.8'	9.00	[c]5.188	72°44.1'
	6.649t	46°54.8'		5.200h	
3.50	4.412h	53°59.7'		5.927	72°51.0'
	7.000t	53°59.7'		6.364t	
4.00	4.647h	59°41.6'		[c]6.457	73°49.6'
	7.000t	59°41.6'		[c]7.000	74° 8.9'
4.50	4.792h	63°43.3'	9.50	[c]5.188	71°32.5'
	7.000t	63°43.3'		5.198h	
5.00	4.888h	66°36.1'		5.927	72°12.7'
	7.000t	66°36.1'		6.037t	
5.50	4.983h	68°59.5'		[c]7.000	74°24.7'
	7.000t	68°59.5'	10.00	[c]5.188	70° 1.1'
6.00	5.078h	70°29.9'		5.195h	
	7.000t	70°29.9'		5.710t	
6.50	5.176h	71°42.6'		[c]5.927	71°33.2'
	7.000t	71°42.6'		[c]7.000	74°37.4'
7.00	5.248h	72°29.8'	10.50	[c]5.188	68°20.4'
	7.000t	72°29.8'		5.190h	
7.50	[c]5.188	73°47.5'		5.384t	
	5.270h	73°47.5'		[c]7.000	74°49.2'
	5.927	73°47.5'	11.00	[c]5.188	66°34.4'
	6.457	73°47.5'		[c]7.000	75° 0.0'
	7.000t	73° 2.2'			

[a]The blade root begins at z = 0, becomes nonradial at z = 9.635 in., and ends at z = 10.80 in. The section at r = 5.927 in. begins at z = 2.276 in., becomes nonradial at z = 8.390 in., and ends at z = 9.674 in. The section at r = 6.457 in. begins at z = 2.804 in., becomes nonradial at z = 7.510 in., and ends at z = 8.854 in. The tip begins at z = 3.351 in., becomes nonradial at z = 6.624 in., and ends at z = 8.026 in.

[b]The symbols h and t indicate hub and blade tip radii, respectively.

[c]These dimensions are for blade template layout only.

[redacted]

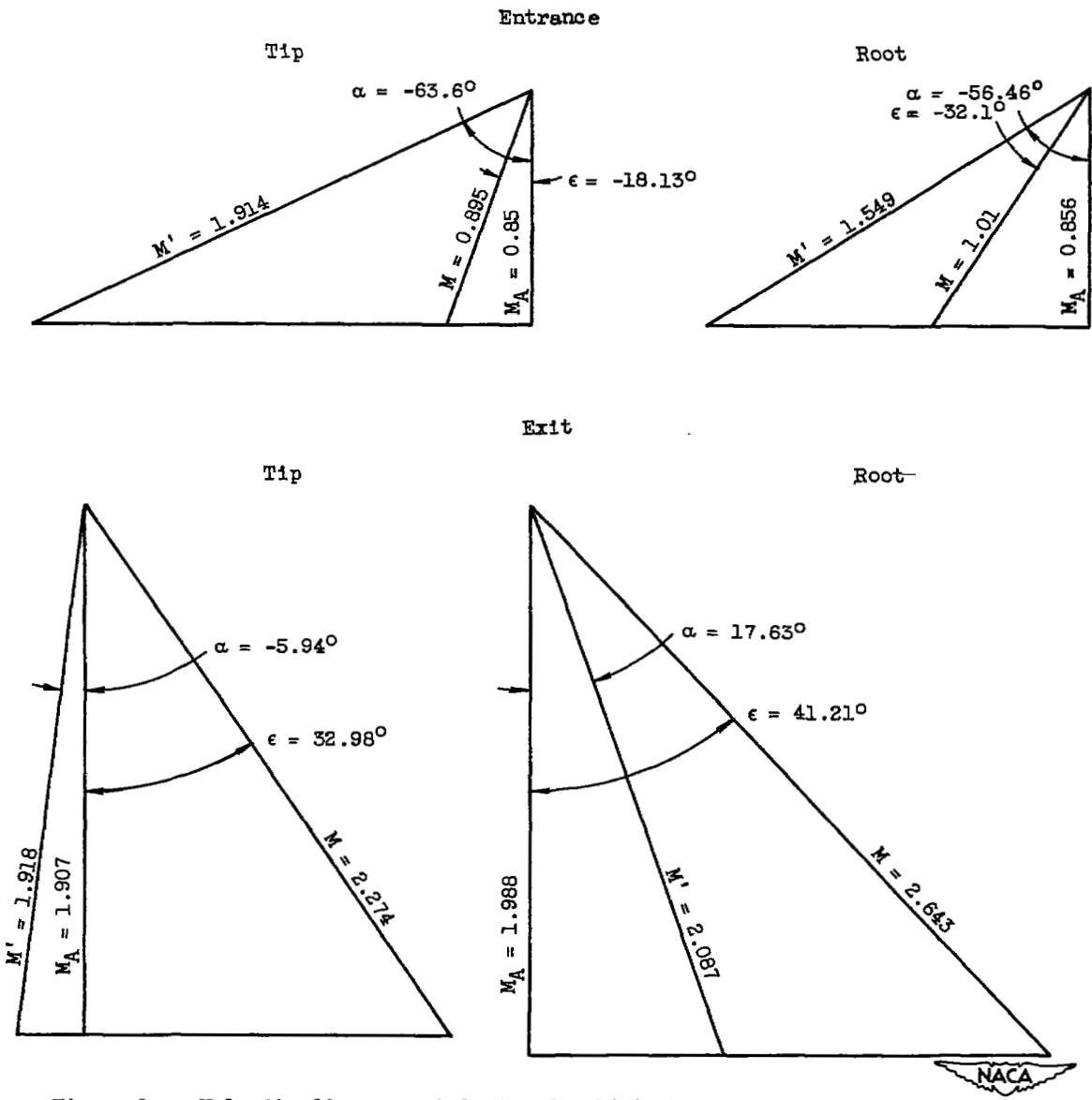

Figure 1. - Velocity diagrams at design for 14-inch supersonic compressor rotor.

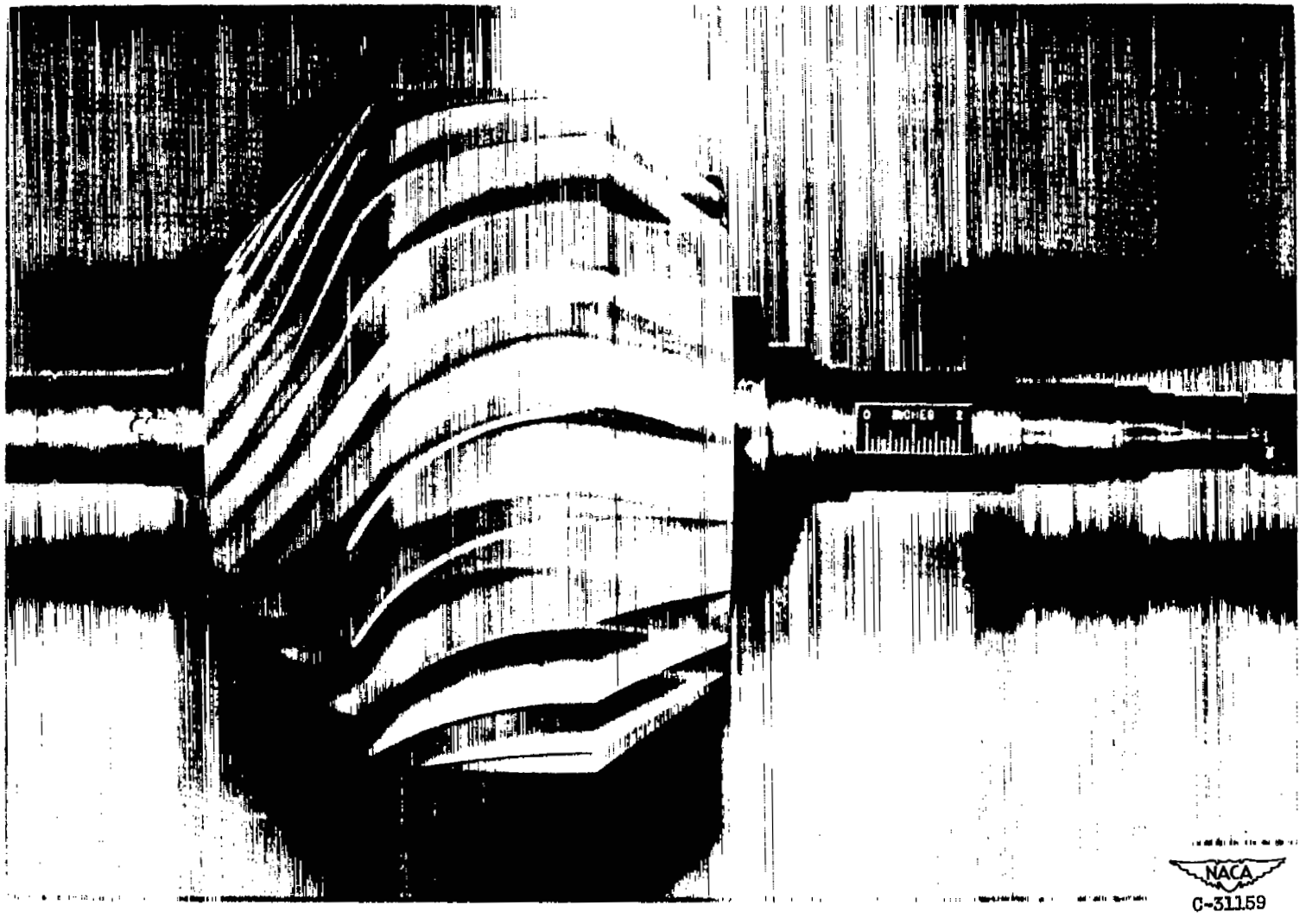

Figure 2. - 14-inch supersonic axial-discharge mixed-flow compressor rotor.

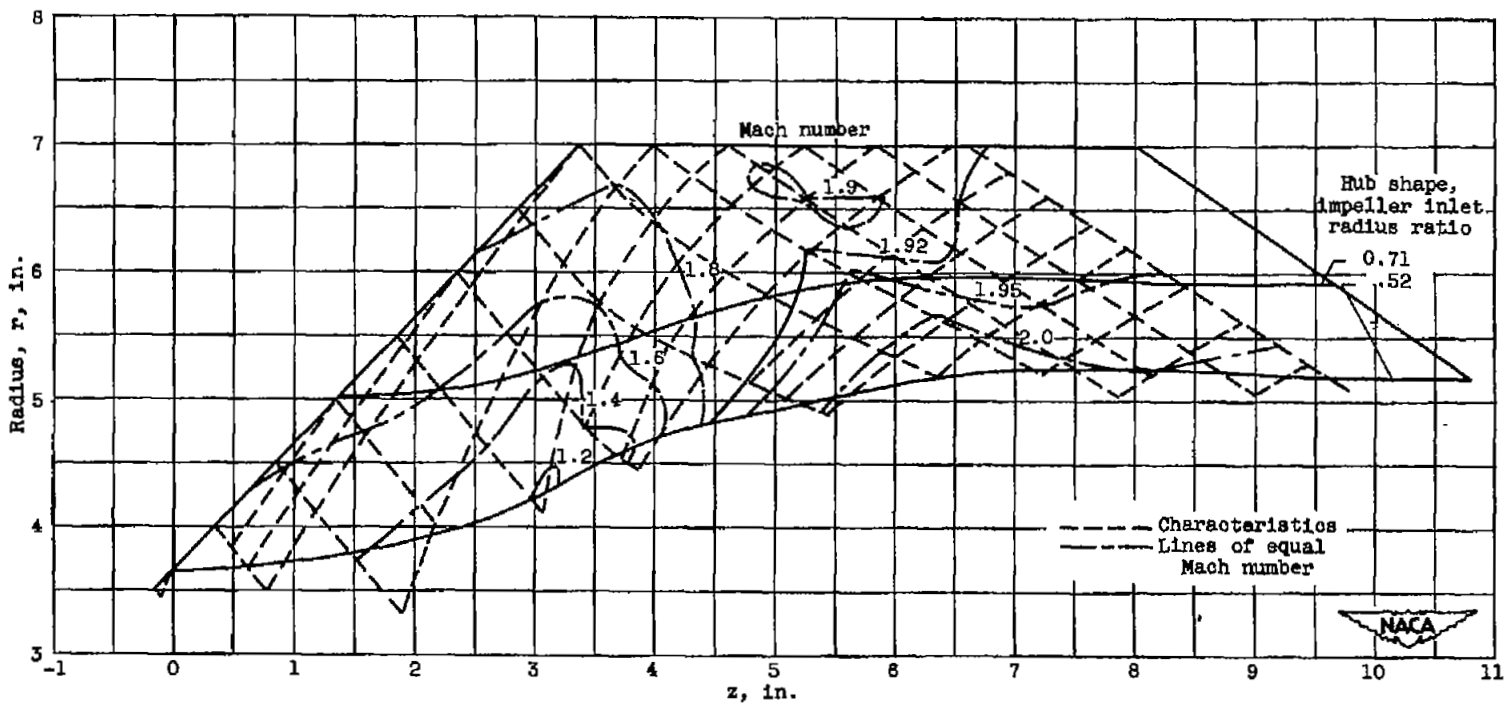

Figure 3. - Sketch of design characteristic network and Mach number contours for 0.52 and 0.71 inlet radius ratio impellers.

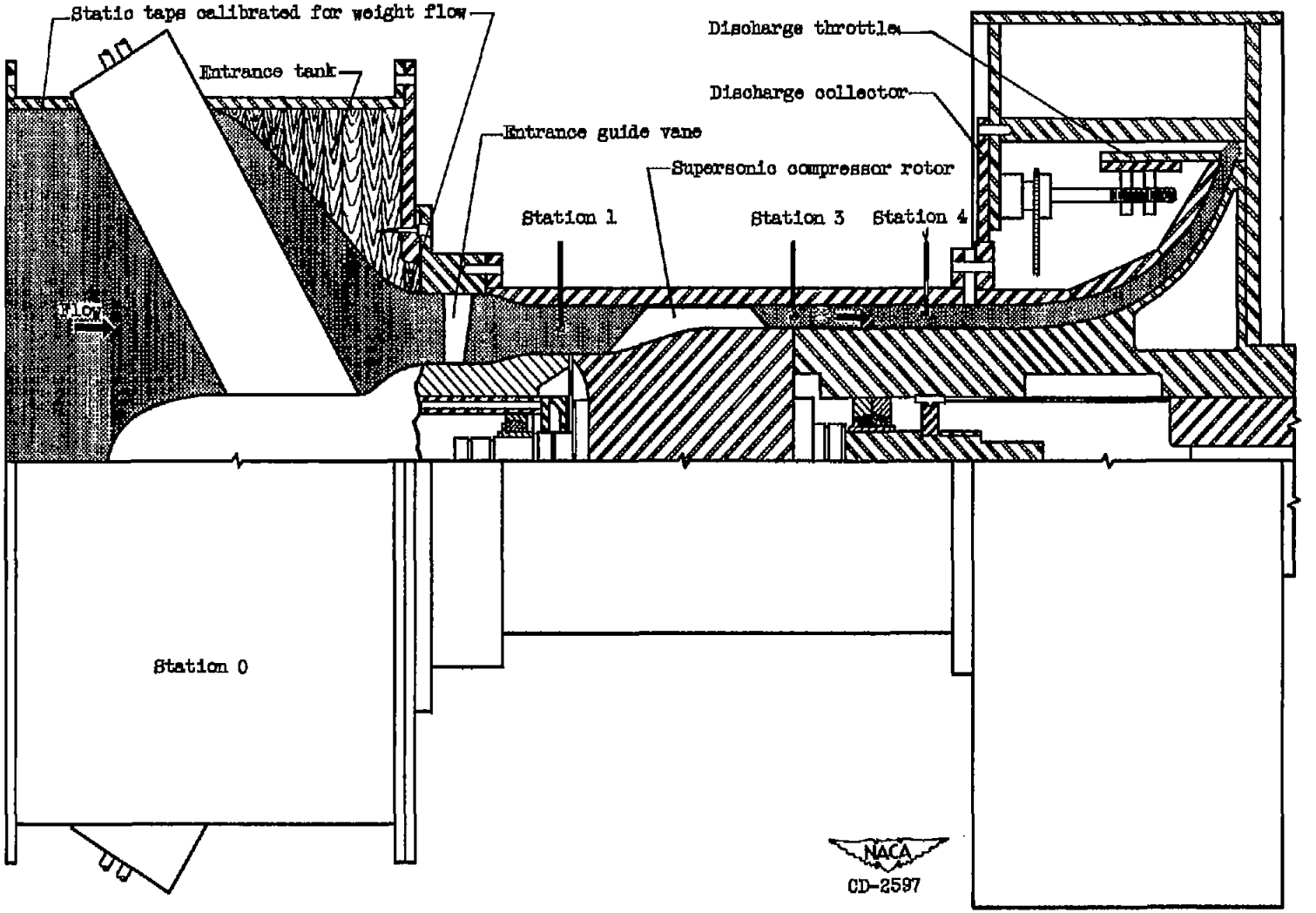

Figure 4. - Schematic diagram of 14-inch supersonic test rig showing 0.72 inlet radius ratio rotor in place.

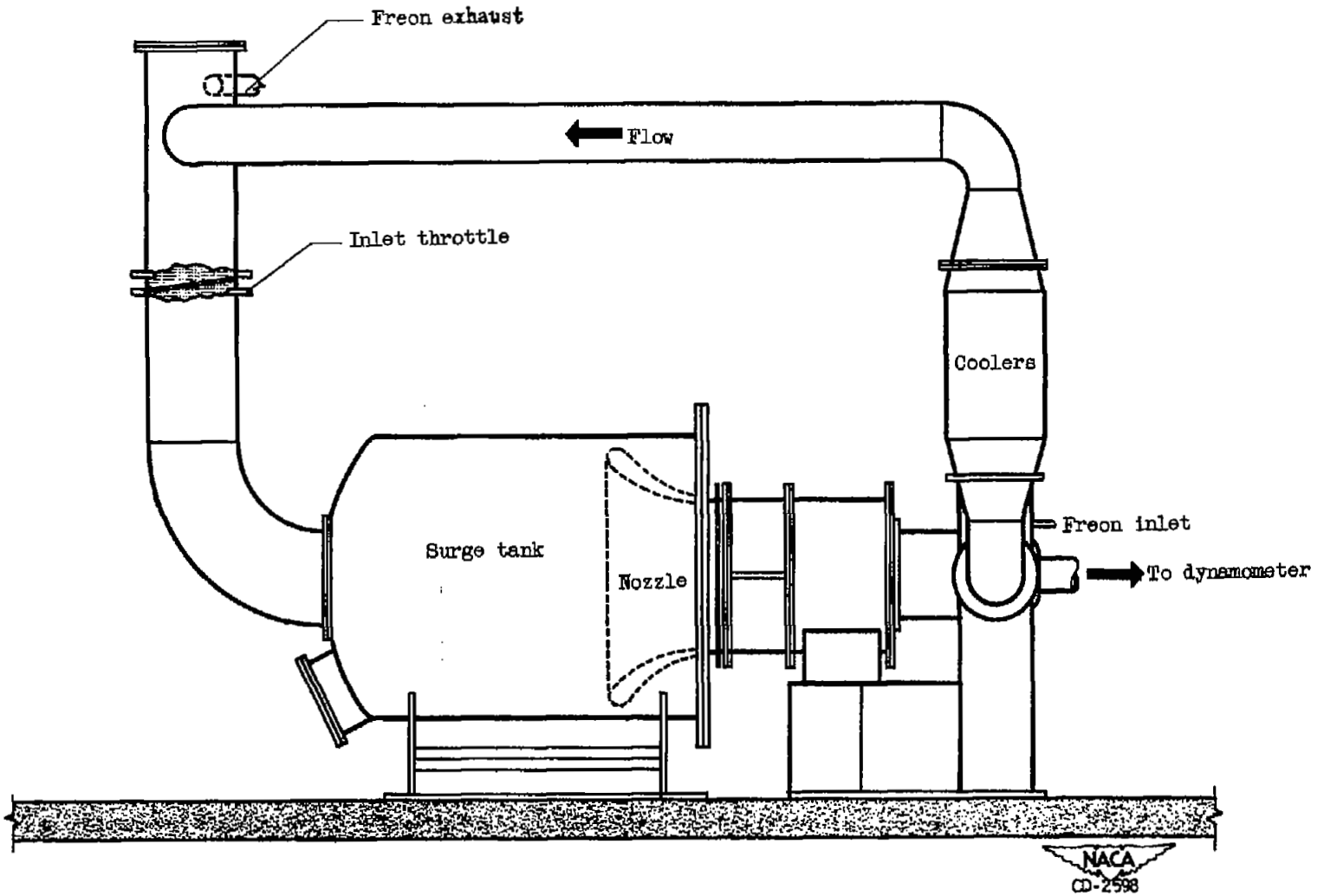

Figure 5. - Schematic diagram of piping assembly and compressor installation.

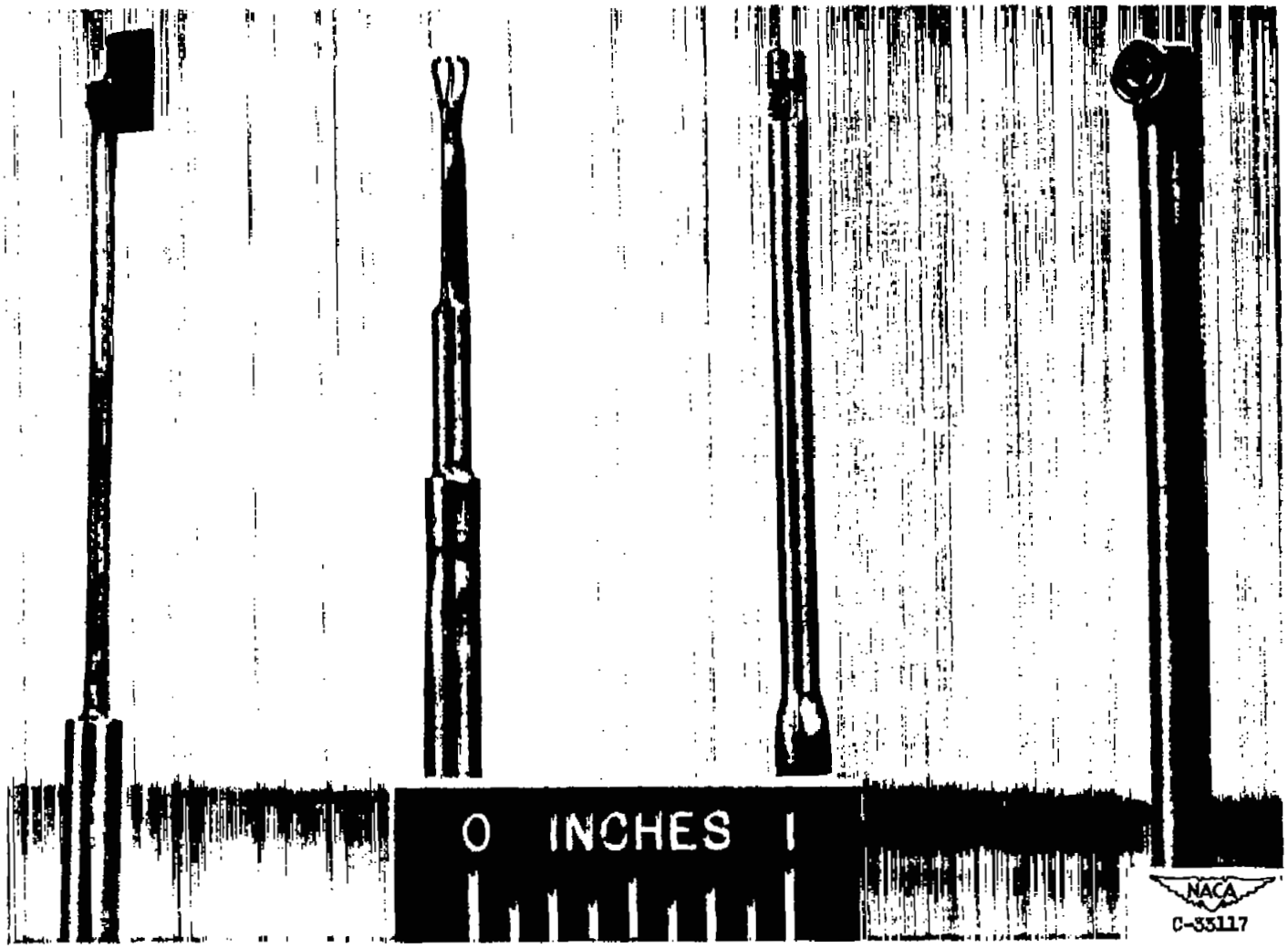

(a) Wedge. (b) Claw. (c) Semishielded thermocouple. (d) Double-shielded thermocouple.

Figure 6. - Exit-survey instruments used in investigation.

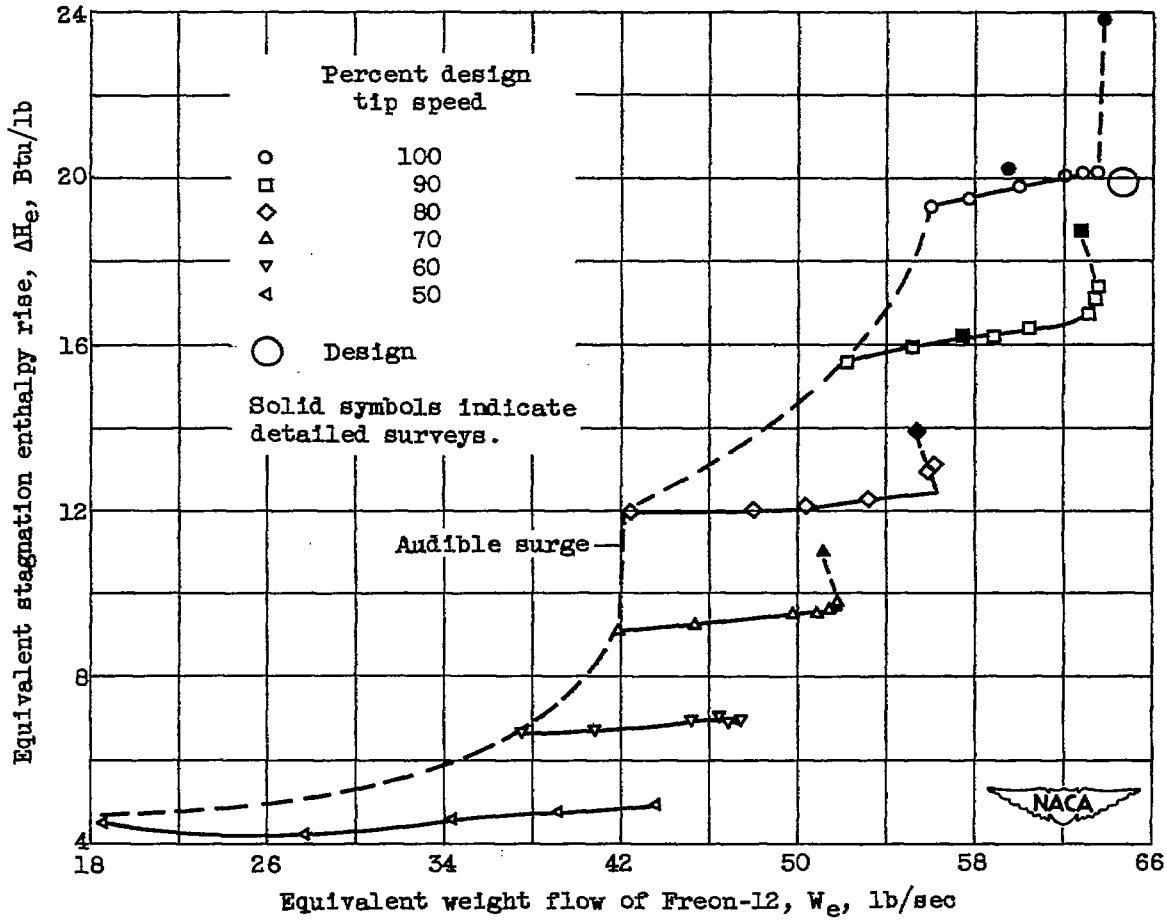

(a) Equivalent stagnation enthalpy rise.

Figure 7. - Performance characteristics for 14-inch supersonic compressor rotor with 0.52 inlet radius ratio.

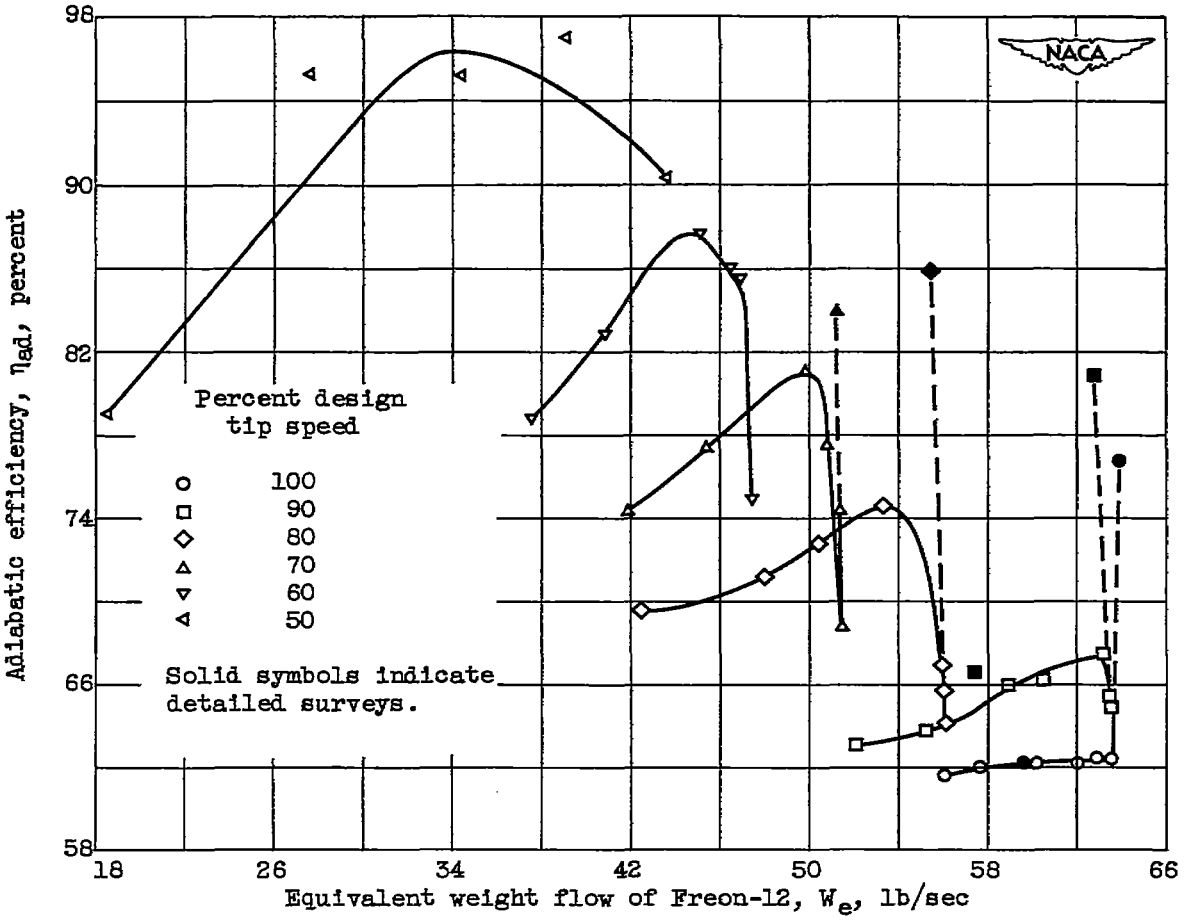

(b) Adiabatic efficiency.

Figure 7. - Continued. Performance characteristics for 14-inch supersonic compressor rotor with 0.52 inlet radius ratio.

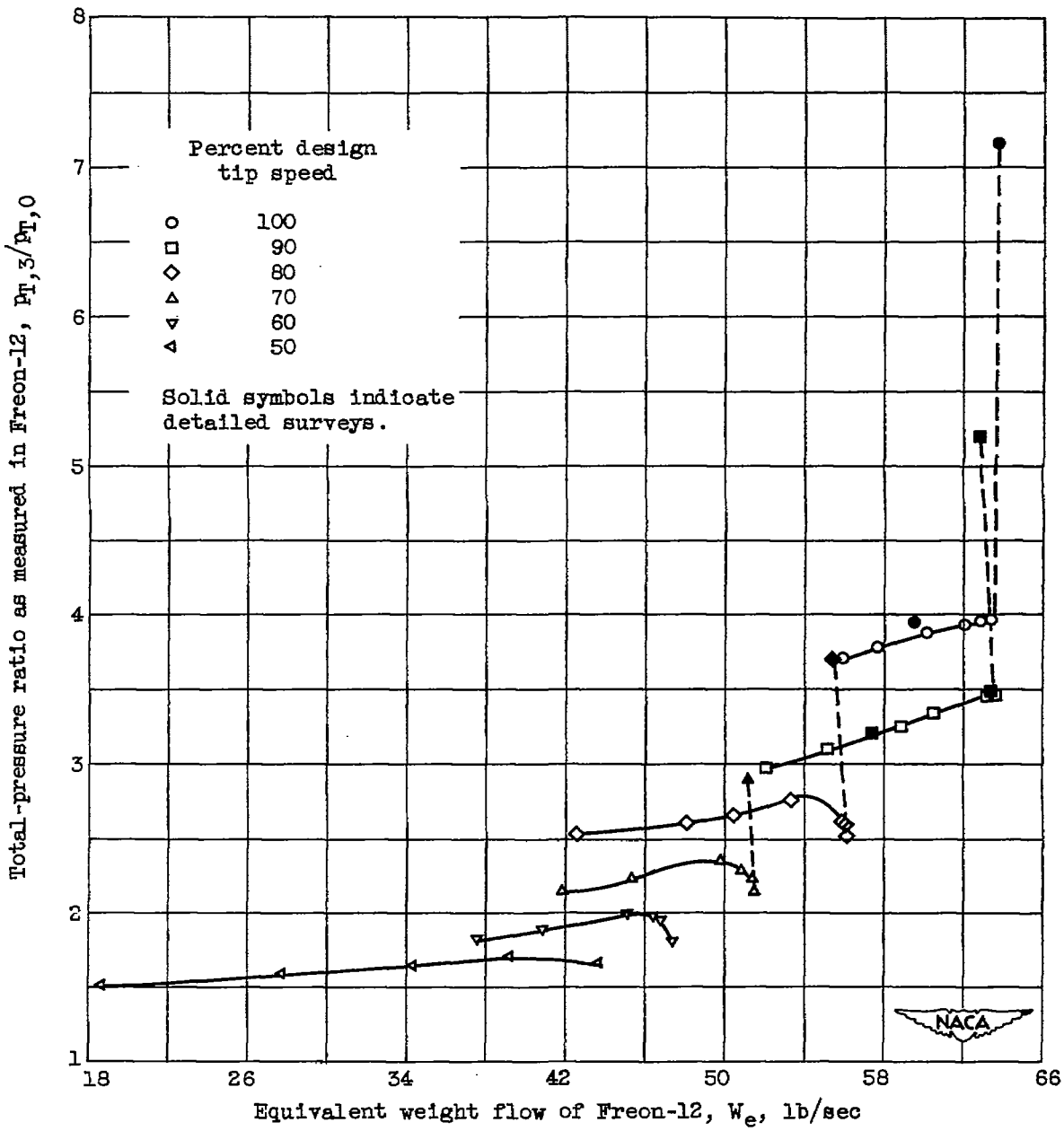

(c) Total-pressure ratio.

Figure 7. - Concluded. Performance characteristics for 14-inch supersonic compressor rotor with 0.52 inlet radius ratio.

[redacted]

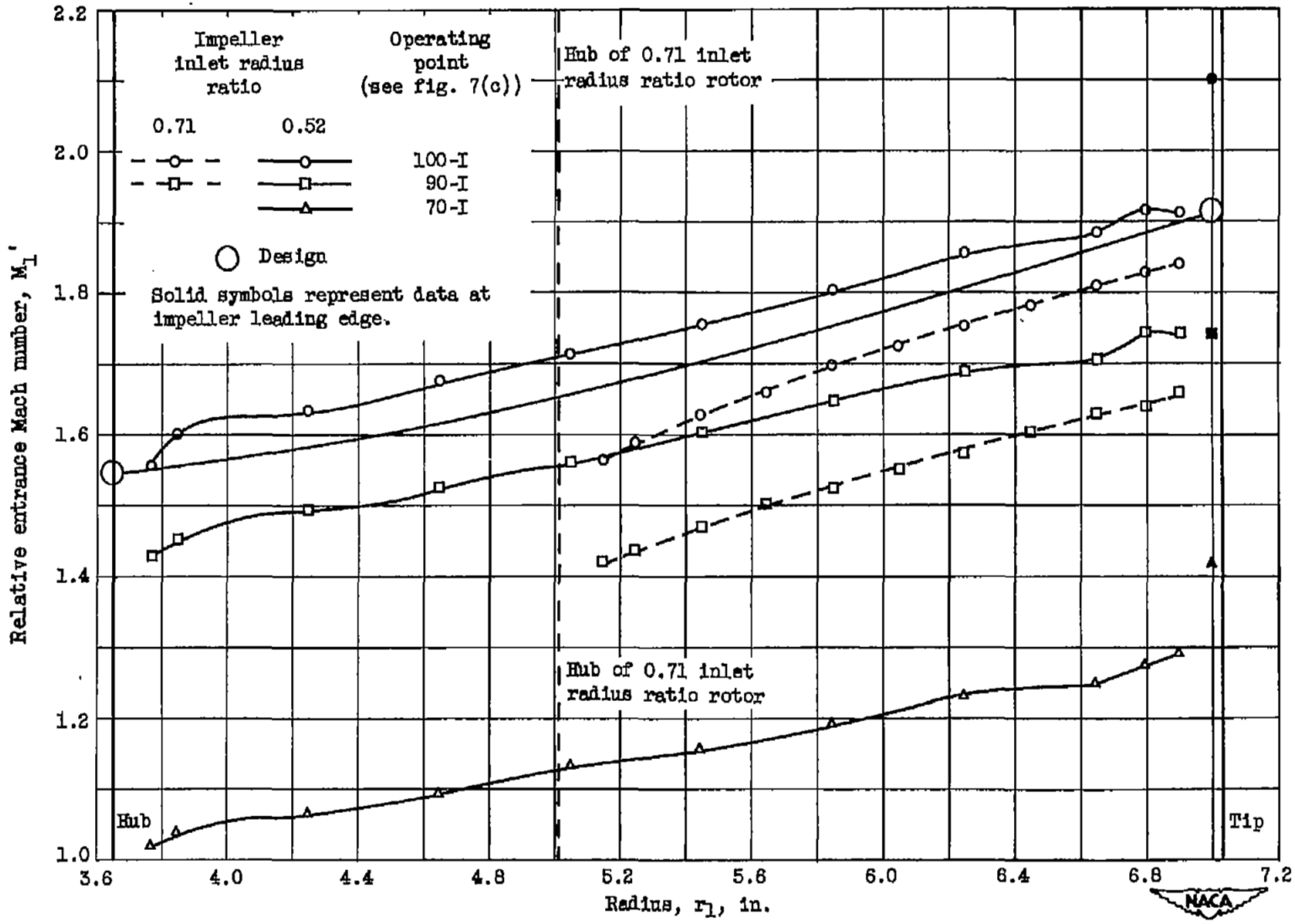

(a) Relative entrance Mach number.

Figure 8. - Conditions (at station 1) upstream of 14-inch supersonic compressor rotor for various speeds.

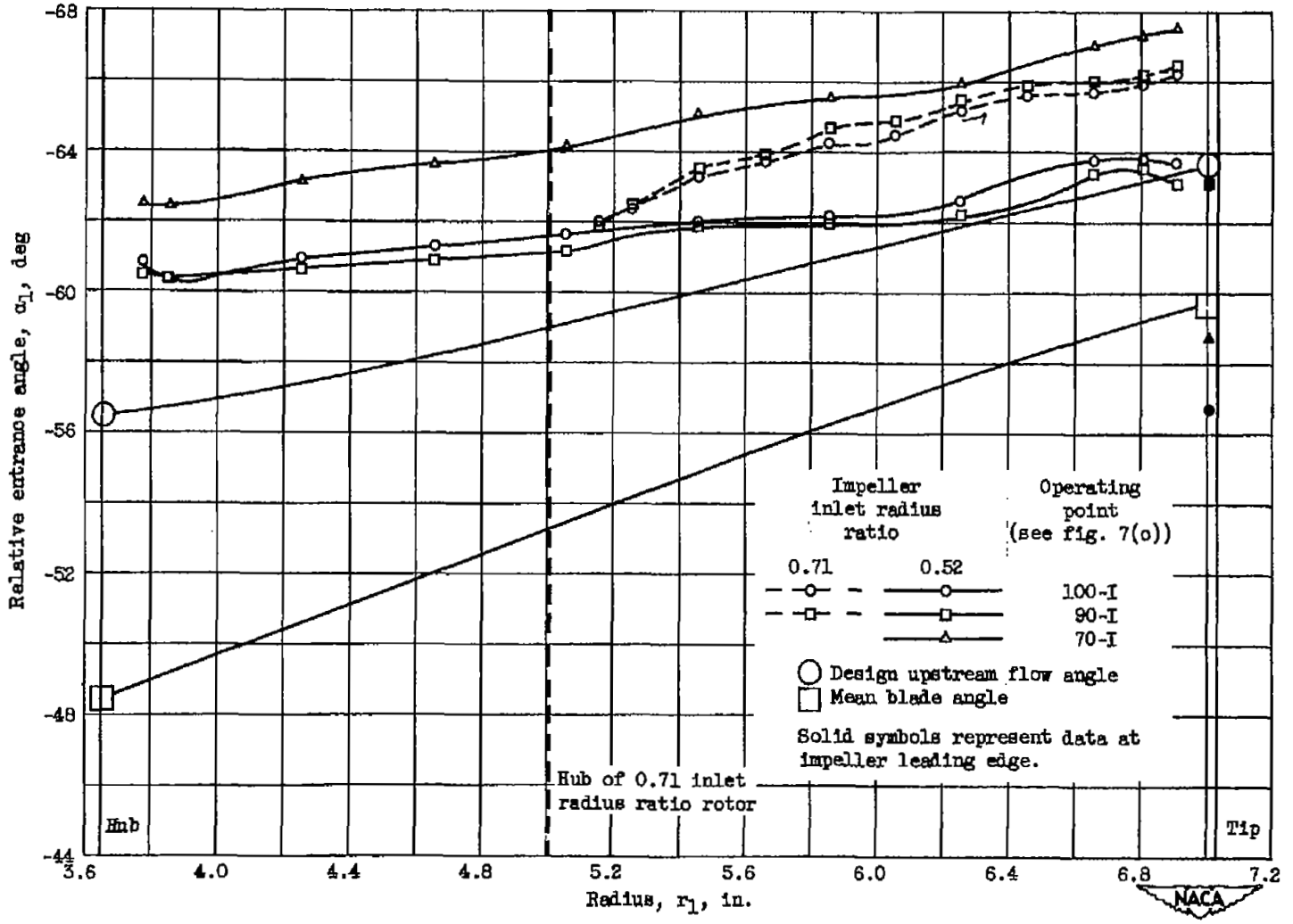

(b) Relative entrance angle.

Figure 8. - Concluded. Conditions (at station 1) upstream of 14-inch supersonic compressor rotor for various speeds.

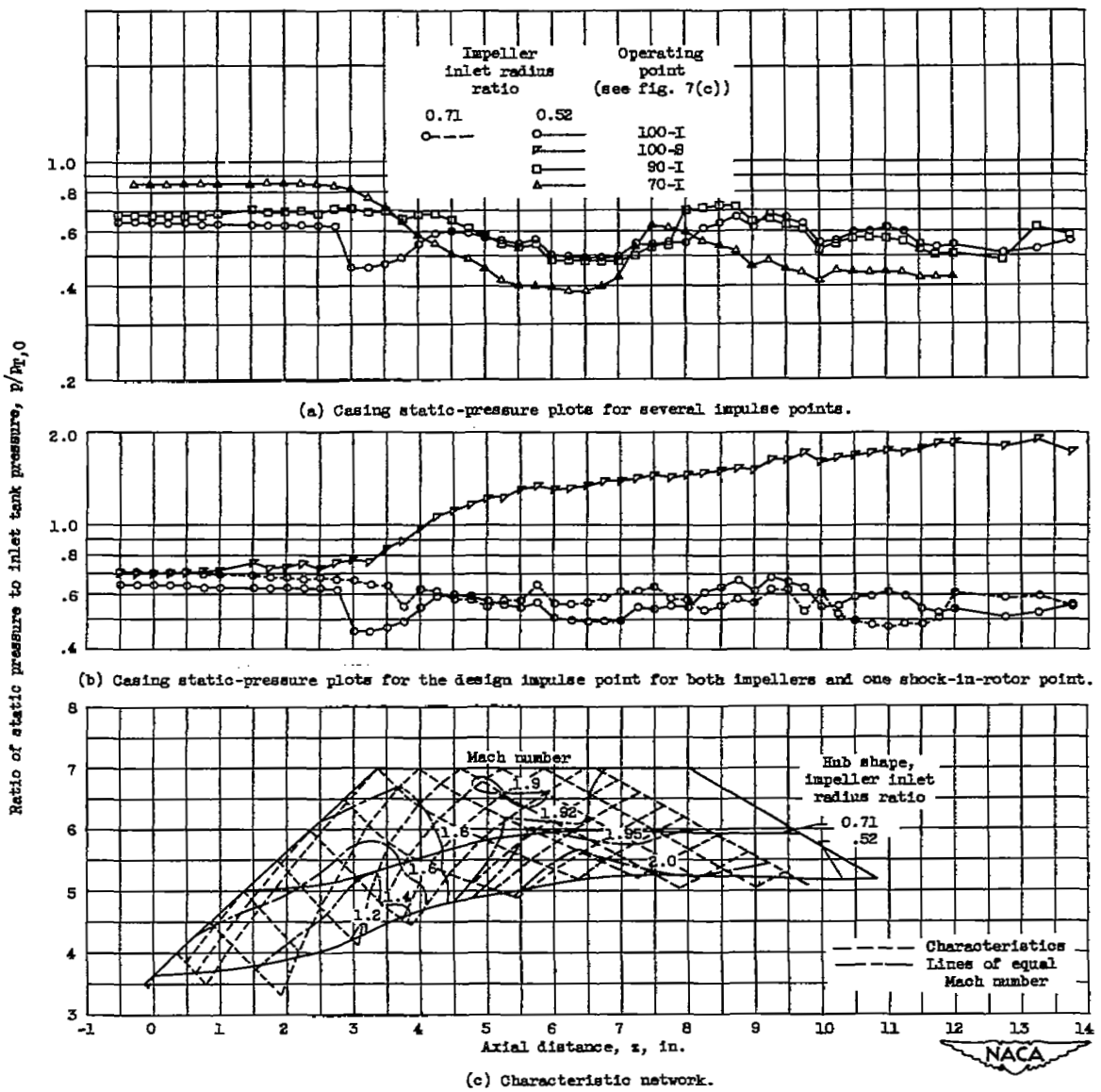

(a) Casing static-pressure plots for several impulse points.

(b) Casing static-pressure plots for the design impulse point for both impellers and one shock-in-rotor point.

(c) Characteristic network.

Figure 9. - Static-pressure distribution along casing of impeller for several operating points.

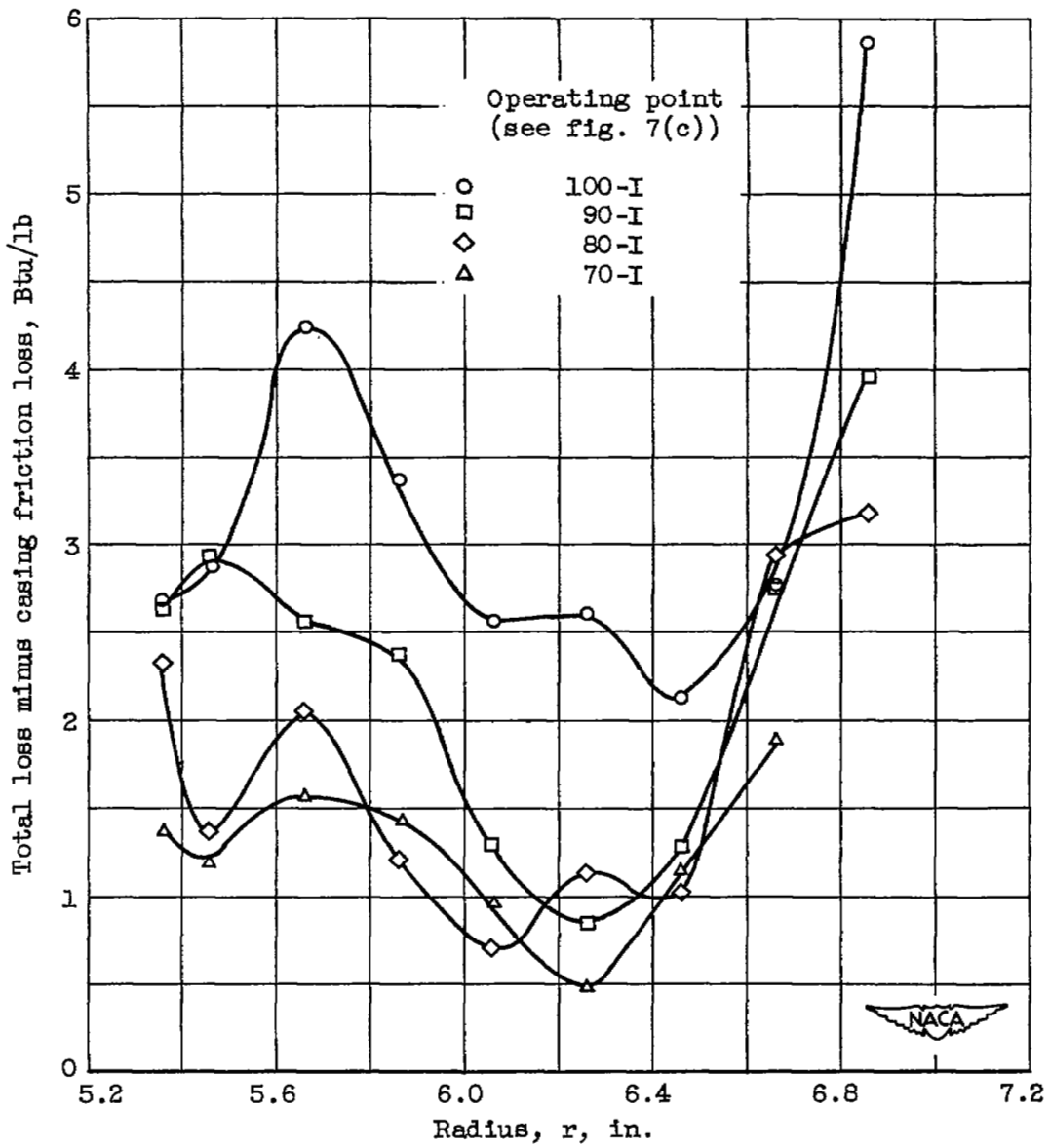

(a) Loss distribution.

Figure 10. - Conditions (at station 3) downstream of 14-inch supersonic compressor rotor for various speeds.

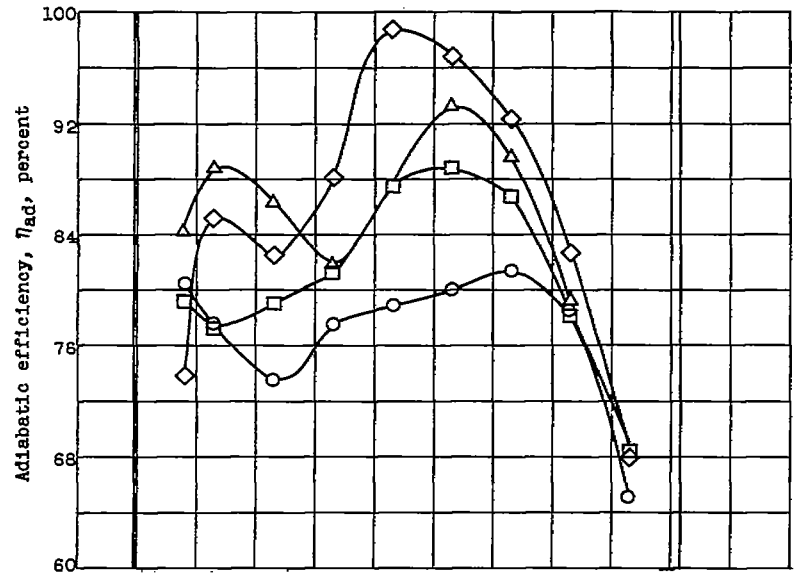

(b) Adiabatic efficiency distribution.

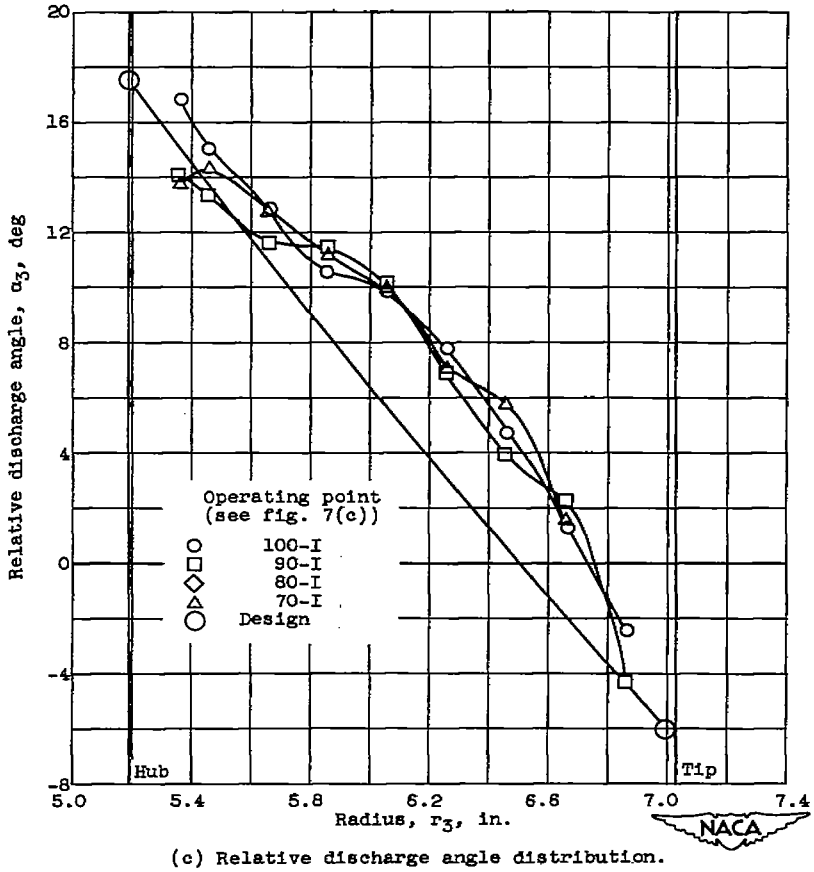

(c) Relative discharge angle distribution.

Figure 10. - Continued. Conditions (at station 3) downstream of 14-inch supersonic compressor rotor for various speeds.

[redacted]

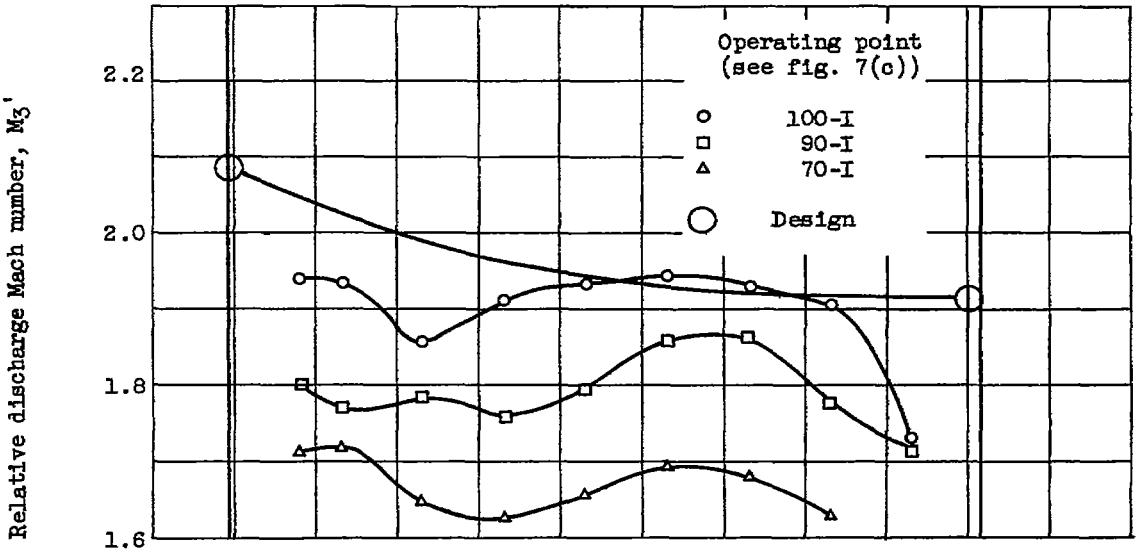

(d) Relative discharge Mach number distribution.

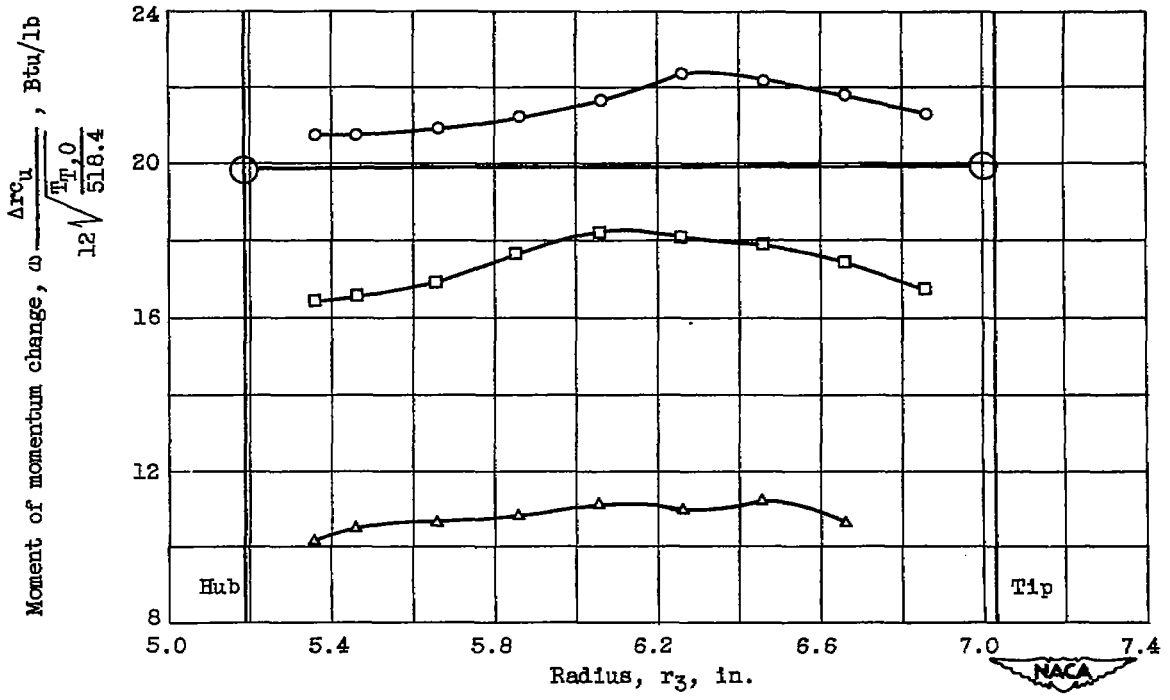

(e) Moment of momentum change distribution.

Figure 10. - Concluded. Conditions (at station 3) downstream of 14-inch supersonic compressor rotor for various speeds.

[redacted]

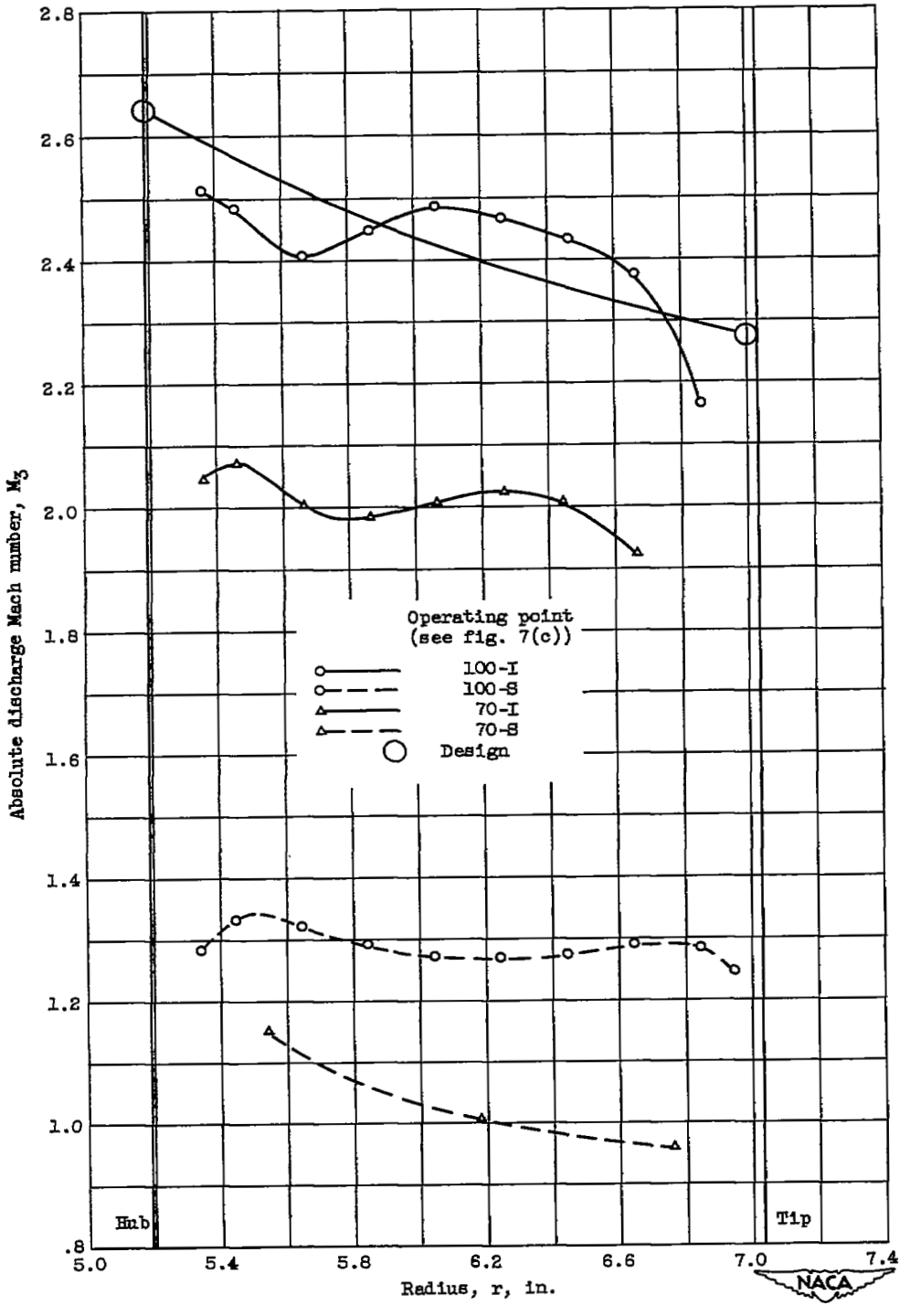

(a) Absolute discharge Mach number.

Figure 11. - Conditions (at station 3) downstream of rotor.

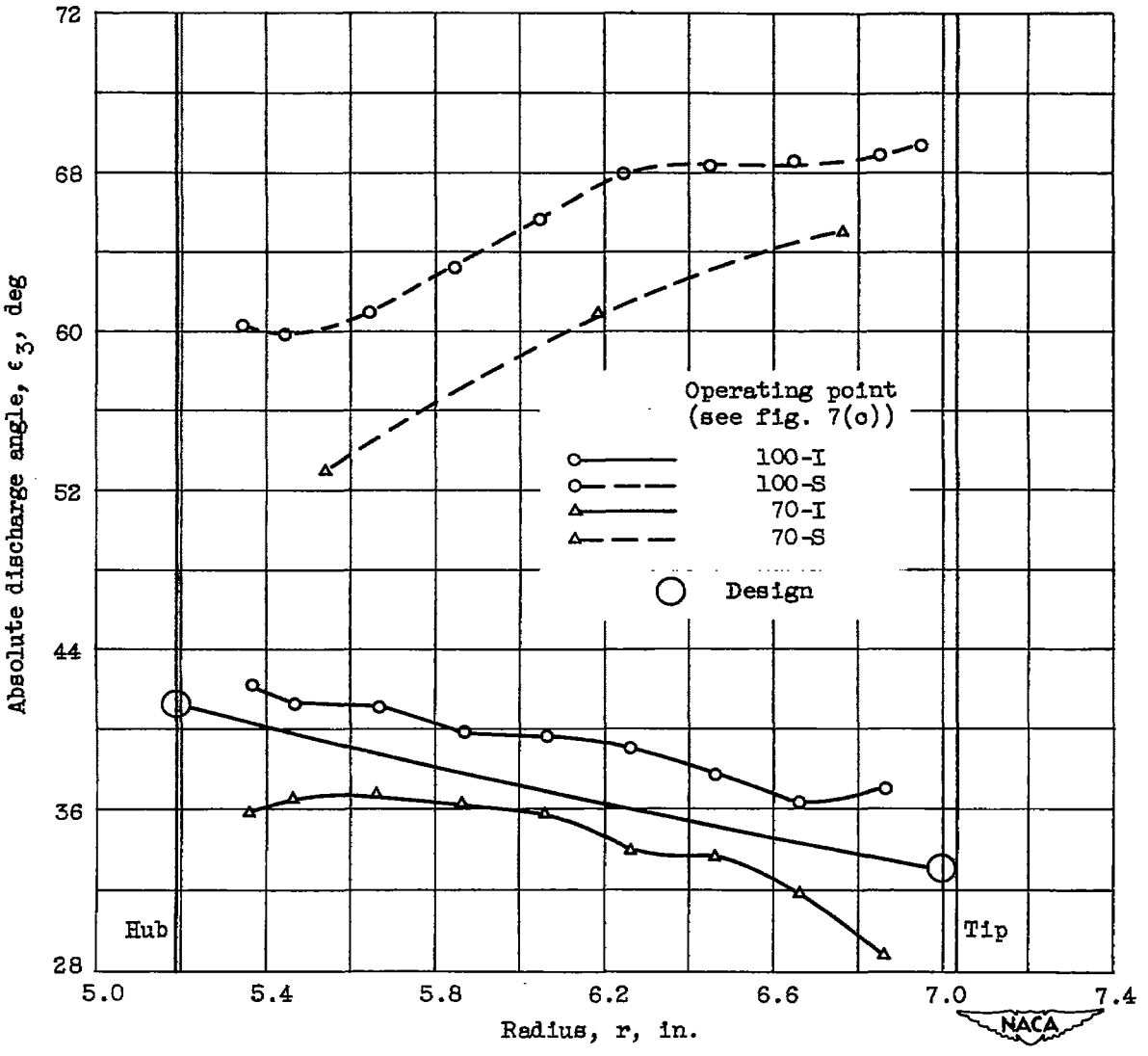

(b) Absolute discharge angle.

Figure 11. - Concluded. Conditions (at station 3) downstream of rotor.

[redacted]